Dyes and Pigments 125 (2016) 375–383

Contents lists available at ScienceDirect

Dyes and Pigments

journal homepage: www.elsevier.com/locate/dyepig

Preparation of a La/N co-doped TiO_2 film electrode with visible light response and its photoelectrocatalytic activity on a Ni substrate

Xiao Zhou [a, c, e], Xiaona Zhang [b], Xinbin Feng [e], Juan Zhou [d], Shaoqi Zhou [a, b, c, *]

[a] Institute of Biology, Guizhou Academy of Sciences, Shanxi Road 1, Guiyang, 550001, PR China
[b] College of Environment and Energy, South China University of Technology, Guangzhou Higher Education Mega Center, 510006, PR China
[c] State Key Laboratory of Subtropical Building Sciences, South China University of Technology, Guangzhou, 510641, PR China
[d] College of Chemical Biology and Material Science, East China Institute of Technology, Guanglan Road No. 418, Nanchang, 330013, PR China
[e] Institute of Geochemistry, Chinese Academy of Sciences, Naming Road No. 46, Guiyang, 550001, PR China

ARTICLE INFO

Article history:
Received 18 July 2015
Received in revised form
27 October 2015
Accepted 29 October 2015
Available online 6 November 2015

Keywords:
La/N co-doping
TiO_2
Ni foam substrate
Photoelectrocatalysis
Visible light
Mechanistic considerations

ABSTRACT

To prevent the recombination of photoelectron–hole pairs and to extend the adsorption in the visible-light region, a TiO_2 coating co-doped with lanthanum and nitrogen on nickel foam was successfully prepared through sol–gel and dip coating methods using the precursors butyl titanate (TBOT) for Ti, lanthanum trioxide for La and urea for nitrogen. The photoelectrocatalytic properties of the prepared samples in the degradation of malachite green were examined under visible light. The phase composition, crystalline structure and optical properties of the La/N co-doped TiO_2(Ni) photo-electrodes were studied using different measurement methods, including XRD, SEM, UV–vis DRS, Raman and FTIR. The results indicated that the co-doped TiO_2(Ni) photo-electrode not only effectively restrained the growth of the TiO_2 grains, but also inhibited the transformation of the titania phase from anatase to rutile. The photo-response of the modified samples was substantially extended from 400 nm to 480 nm, and the band gap narrowed from 3.2 eV to 2.79 eV. The co-doped TiO_2(Ni) samples exhibited higher photocatalytic activity as a result of the synergistic effects of the La and N co-doping. The degradation rate of malachite green by the $La_{0.2\%}N_{20\%}/TiO_2$(Ni) photo-electrode was 23.5% higher than that of the un-doped sample; this result indicated that the extended range of responsive wavelengths greatly expanded the possible applications of the modified electrode. When a low bias voltage was applied to the $La_{0.2\%}N_{20\%}/TiO_2$(Ni) photo-electrodes, the electrodes exhibited even better photoelectrochemical properties and photoelectrocatalytic activity than a $La_{0.2\%}N_{20\%}/TiO_2$(Ni) film under visible light irradiation.

1. Introduction

Titanium dioxide has proven to be one of the most promising photocatalysts for environmental applications, including as solar cells, in hydrogen production and for the decomposition of organic pollutants, because of its high photocatalytic activity, better chemical stability against corrosion, lack of toxicity and economic availability [1]. TiO_2 exists in three different crystalline forms: anatase, rutile and brookite. The anatase form is the most active and most commonly applied form of TiO_2. However, the photocatalytic efficiency of titanium dioxide is limited by its low efficiency for visible light utilization because of its wide band gap(3.2 eV) [2] and the high recombination rate of its photogenerated electron–hole pairs [3]; additionally, the need to separate suspended TiO_2 particles from water prevent the application of TiO_2 in water treatment. To enhance the photocatalytic activity in the visible light region toward the degradation of different pollutants, many approaches, such as surface modification, structure optimization, and doping with metal or non-metal elements, have been developed to solve these problems.

In recent years, the doping of TiO_2 by cations and/or anions has been the subject of many studies [4–13]. Recently, TiO_2 co-doped with rare earth and non-metal elements has greatly aroused our interest. Many reports show that TiO_2 co-doped with rare earth and non-metal elements has better photocatalytic performance because of the synergistic effects of the co-doping. According to the previous work, the synergistic effects of co-

* Corresponding author. College of Environment and Energy, South China University of Technology, Guangzhou Higher Education Mega Center, 510006, PR China. Tel.: +86 2039380579.
E-mail address: fesqzhou@scut.edu.cn (S. Zhou).

http://dx.doi.org/10.1016/j.dyepig.2015.10.044
0143-7208/

doped TiO_2 are as follows: (1) In TiO_2, rare earth elements can substitute for $Ti^{4+}$and can enable the separation of photo-generated electron–hole pairs. Lanthanum ions have a special $4fx5dy$ electronic structure that can form complexes with various Lewis bases and can improve the conversion efficiency of TiO_2. As more organic molecules are adsorbed on the surface of the TiO_2 [10,14–16], its absorption characteristics increase and the recombination rate for electron–hole pairs decreases. As a result, the TiO_2 is more feasible for photocatalysis under visible light. (2) Several works reported that doping anatase TiO_2 with an anion, such as N [13] or S [12], can narrow the band gap of TiO_2 and can improve the quantum yield through the mixing between the p states of N or S with the O 2p states of the O_2 in the TiO_2 lattice. Consequently, anion doping improves the optical response of TiO_2 by shifting the response from the UV to the visible part of the solar spectrum [17,18]. N is considered to be the most promising of the non-metal dopants because the ionic radius of N is close to that of O and the N 2p states can effectively merge with the O 2p states [19,20]. Although doping TiO_2 with an anion can effectively enhance the photocatalytic activity in visible light, the recombination centres of the partially occupied impurity bands caused by mono-doping inhibit the transfer of light-induced charge carriers to the surface of TiO_2; this inhibition reduces the photo-generated current [21–23]. This drawback can be solved by doping the TiO_2 with rare earth elements because this doping causes the formation of a new energy level between the TiO_2 valence and conduction bands, oxygen vacancies, etc. Doping with rare earth elements can significantly reduce the recombination rate of the photoelectron–hole pairs and can enhance the interfacial charge-transfer efficiency.

Several research groups have fabricated TiO_2 on glass, Ti plates [24] and activated carbon fibre substrates [25]. The electron transfer between the TiO_2 film and the supporting substrate can affect the PEC efficiency when a bias potential is applied [26]. Foamed nickel plates which have many microscopic open cages and a high work function of 5.1 eV, are a promising material for preparing TiO_2 film electrodes because of their good electric conductivity, large surface area and three-dimensional network structure, which is good for the transport of reactants to the surfaces of the electrocatalyst [1].

The dip-coating technique has been popularly used because that it is simple, low cost, less time consuming, cheaper base material and precursors can be used, good control on layer thickness, and less wastage during fabrication of both porous and dense coatings [27]. The immersion of substrate in the coating slurry or suspension ensures that most of the material surface is completely coated. Nevertheless, practically TiO_2 films on foam Ni substrates by the dip-coating deposition have rarely reported.

Although the co-doping of TiO_2 with rare earth and non-metal ions can enhance its photo-response to visible light and the immobilization of TiO_2 nano-particles onto a substrate can solve the problem of recycling, this approach leads to decreases in the surface area and the quantum efficiency [28,29]. Furthermore, the fast recombination of photo-generated electron-/hole (e^-/h^+) pairs still causes problems [30]. Therefore, it is important to retard the recombination of the charge carriers. Vinodgopal [31] reported that 4-chlorophenol (4-CP) was efficiently degraded by a TiO_2 thin film electrode under UV irradiation. Great interest in photo-electrocatalysis (PEC) has been emerging. The PEC process combines electrochemical and photocatalytic technologies. The process promotes the separation of photo-generated electron–hole (e^-/h^+) and prevents their recombination through electron transfer controlled by an external circuit. At present, PEC using TiO_2 photocatalysts has been widely applied to the degradation of recalcitrant organic pollutants because of PEC's enhancement of the photocatalytic efficiency [32]. PEC in which a positive potential is applied to the TiO_2 shows enhanced quantum efficiency and increased degradation rates of the recalcitrant pollutant. Application of potential across the immobilized TiO_2 is a key factor that prevents the high recombination rate of the photo-generated electron–hole pair and enhances the quantum efficiency of this process.

To the best of our knowledge, there have been no reports on the synthesis of La- and N- doped TiO_2 coatings on nickel foam substrates or on their photoelectrocatalytic performance toward the degradation of organic pollutants.

In this work, we prepared La_xN_y co-doped TiO_2 coatings on nickel foam by sol–gel and dip coating methods. The photocatalytic and photoelectrocatalytic activities of the prepared samples were investigated through the degradation of malachite green under irradiation by visible light. The synergistic effects of co-doping TiO_2 with lanthanum and nitrogen were studied in detail. Several potential biases were applied between the La_xN_y co-doped TiO_2(Ni) electrode and the counter electrode (a graphite rod) to promote migration of photo-generated electrons to the counter electrode through the outer circuit and to prevent the recombination of electrons and holes. Moreover, the stability of the La_xN_y co-doped TiO_2(Ni) electrode toward the degradation of MG was analysed in detail.

2. Experimental

2.1. Materials

Porous nickel was chosen as the Ni substrate (purity >99.5%, porosity>95%, 300 mm × 210 mm × 4 mm) from LiFeixin Environmental Protection Equipment Corporation (Shenzhen, China). Lanthanum trioxide (purity > 99.7%) was purchased from Zhujiang smelter (Guang Zhou, China). Malachite green (MG) and urea were purchased from DaMao chemical regent factory (TianJin, China), and all of the chemicals were of analytical purity.

2.2. Preparation of La/N co-doped TiO_2(Ni) electrodes

A large sheet of raw porous nickel with a thickness of 4 mm was cut into small rectangular pieces 50 mm × 80 mm, which were ultrasonically cleaned in an alcohol and acetone solution followed by washing with distilled water. The La/N co-doped TiO_2 was synthesized using a sol–gel method. In a typical synthesis, the two components (A and B) were first prepared separately at first. For component A, 15 mL of butyl titanate was added to 20 ml absolute ethyl alcohol with 10 mL glacial acetic acid at room temperature and was stirred for 30 min. Component B consisted of 10 mL of acetic acid, ultrapure water, 25 ml of absolute ethyl alcohol and urea and lanthanum trioxide, which served as dopants; the mole ratios of lanthanum trioxide and urea were $n(La):n(N):n(Ti) = x:y:1$, x = 0.05%, 0.10%, 0.15% and 0.20%, y = 15%, 20%, 25% and 30%, respectively. Then, component A was added drop-wise into component B under vigorous stirring at a dropping rate of 12 drops per second. The mixture was stirred for another 60 min and was aged 2 h to obtain a gel at room temperature.

The La_xN_y co-doped TiO_2(Ni) film electrode was prepared by the dip-coating method because of the method's low cost and controllability. A porous nickel sheet was cleaned, was dipped horizontally into the gel for a certain time, was then raised at a certain speed and was dried under an electric heat drum wind drying oven for 20 min to form a film. The film electrodes were annealed at 500 °C for 180 min in a muffle furnace after dip-coating 5 times to guarantee complete coverage by the coating layer. Finally, the La_xN_y co-doped TiO_2(Ni) film electrode was used after it

cooled. Before the La_xN_y/TiO_2/Ni film electrode was used for the photoelectrocatalytic study, its structural and surface morphology were examined and studied using X-ray diffraction, Raman spectroscopy, UV–vis/DRS and scanning electron microscopy (SEM).

2.3. Photoelectrocatalytic reactor and light source

The photoelectrocatalytic oxidation experiment was performed in a photoelectrocatalytic reactor system. The components of the reactor were described precisely in our previous study [33]. The PEC reactor consisted of a cylindrical glass beaker, a 50 W tungsten halogen lamp (EXZ MR16 SP, GE, USA), a digital DC power supply (SS1792C, SUING, Shijiazhuang) and electrodes. The 50 W tungsten halogen lamp was positioned inside the cylindrical beaker surrounded by a constant temperature electric water bath to control the temperature. The photo-reactor has an effective volume of 500 ml, in which a La_xN_y/TiO_2/Ni film anode, a carbon stick cathode (Φ10 mm, 80 mm) and a saturated calomel electrode (SCE) were placed in parallel and were connected with the DC power supply. The sample solution was agitated with a magnetic stirrer and was irradiated with visible light. Magnetic stirring at a slow speed was maintained throughout the reaction. During the reaction, 10 ml of the MG solution was removed at given time intervals, and the concentration of MG was analysed at its maximum absorption wavelength of 616 nm.

2.4. Procedure for the PEC degradation experiment

In this study, a total of six sets of tests were performed with different purposes. The first set of tests was conducted under different experimental conditions, including different mole ratios of lanthanum trioxide and urea and different potential bias voltages. All of the photocatalytic and photoelectrocatalytic tests were performed in 60 mL of 0.5 mol/L Na_2SO_4 solution.

For the photoelectrocatalytic activity tests, a tungsten halogen lamp was used as the light source, and the objective degradation pollutant was 500 mL of 30 mg/L MG solution; For the electrocatalytic activity test, different external bias potentials were applied between the working electrode and the counter electrode; The degradation occurred under visible light for 240 min. The PEC and photocatalytic degradation ratio is described by $(1-C_t/C_0) \times 100\%$, where C_0 is the adsorption of solution at its equilibrium concentration, and C_t is the concentration of the solution at time t.

2.5. Analytical methods

X-ray diffraction (XRD) patterns were obtained from a Bruker D8 Advance X-ray diffractometer with Cu K radiation over a 2θ range of 20–70°. The Raman spectra were collected with a HJY Lab RAM Aramis microscopic Raman spectrometer. The UV–vis diffuse reflectance spectra were measured over a wavelength range of 200–600 nm with a SHIMADZU UV2450 UV–vis spectrometer. The morphologies of the La/N co-doped TiO_2 film electrode were observed with a PhilipXL-30 Series Philip scanning electron microscope. The UV absorption of MG in the aqueous solutions was measured with a spectrophotometer (Unico 2800 UV–vis) at 616 nm. The light intensity was 80.1 mW cm^{-2} (380 nm ~ 780 nm), as measured with a Spectrascan spectroradiometer(PR-705, Photo Research, USA). The Fourier transform (FTIR) spectra were measured using a Vector 3 spectrometer (Bruker) with a spectral resolution of 8 cm^{-1} over range of 4000-400 cm^{-1}. The Raman spectra were recorded using a Varian FT-Raman spectrometer over a Raman shift range of 400–4000 cm^{-1}.

3. Results and discussion

3.1. Characterization of the La/N co-doped TiO_2 film electrode

3.1.1. XRD

All of the XRD patterns of the TiO_2 film electrode samples are shown in Fig. 1, in which the pure TiO_2 film electrode exhibited the presence of anatase phase TiO_2 (major peaks: 25.4°(101), 37.0°(103), 37.8°(004), 38.5°(112), 48.0°(200), 54.1°(105) and 55.1°(211)) and the characteristic peaks of the rutile phase (major peaks: 27.4°and 36.1°). However, other crystalline phases, such as La_2O_3, were not observed, and at the lack of these phase signified that the lanthanum ions might have successfully doped the lattice of the TiO_2 or might be interstitially well dispersed on the surface of TiO_2 in quantities too low to be detected by XRD. N-doping did not change the anatase phase of the TiO_2 but inhibited the formation of rutile TiO_2.

An observable and obvious phenomenon is that the presence of dopants leads to weak and broad peaks that indicate a reduction in crystallinity, which is normally associated with reduced particle size. According to the Scherrer equation, $D = R\lambda/\beta \cos\theta$, where D is the crystal size, R is the Scherrer constant, λ is the X-ray wavelength, β is the full width at half maximum and θ is the diffraction angle. The particle sizes for all of the samples were calculated from the XRD data using the Scherrer equation. The calculated results in Table 1 indicated that doping with the lanthanum ion had the effect of refining the grain size; the minimum crystal size was 10.7 nm at La_x:N $_y$ = 0.15%: 20%.

The La and N dopants inhibit the anatase particle growth, and La has more inhibiting power, as can be seen in the graphs because the peaks for the La-doped TiO_2 are less intense and are broader than those for the N-doped TiO_2. These results revealed that the N atoms were incorporated into the crystal lattice of TiO_2. To substantiate this finding, the XRD patterns were acquired for samples with fixed amounts of N (20%) and various amounts of La from 0.05% to 0.2%, and the results are displayed in Fig. 1. An increase in the amount of La in the co-doped TiO_2 also leads to a decrease in the peak intensities and hence a reduction in the particle size. La_2O_3 might form a binary metal oxide with TiO_2. The ionic radius of La^{3+} is 0.136 nm, which is larger than that of Ti^{4+} (0.068 nm), so it is impossible for the La^{3+} ions to actually enter the TiO_2 lattice under the conditions of the sol–gel process. The calculated particle sizes are 12.3 nm, 11.9 nm, 10.7 nm and 11.1 nm for $La_{0.05\%}N_{20\%}$–TiO_2, $La_{0.1\%}N_{20\%}$–TiO_2, $La_{0.15\%}N_{20\%}$–TiO_2

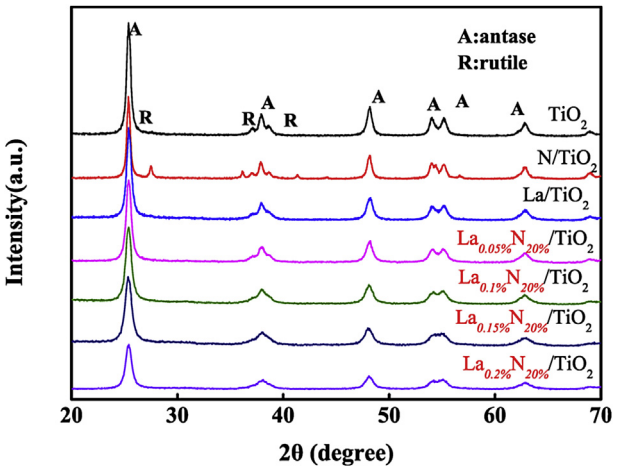

Fig. 1. XRD patterns of $La_{0.05\%}N_{20\%}/TiO_2$, $La_{0.1\%}N_{20\%}/TiO_2$, $La_{0.15\%}N_{20\%}/TiO_2$ and $La_{0.2\%}N_{20\%}/TiO_2$.

Table 1
Particle sizes of the prepared samples calcined at 500 °C, estimated from XRD data.

Samples	Pure TiO_2	$N_{20\%}/TiO_2$	$La_{0.2\%}/TiO_2$	$La_{0.05\%}N_{20\%}$–TiO_2	$La_{0.1\%}N_{20\%}$–TiO_2	$La_{0.15\%}N_{20\%}$–TiO_2	$La_{0.2\%}N_{20\%}$–TiO_2
Estimated crystallite size(nm)	17.1	21.8	15.1	12.3	11.9	10.7	11.1

and $La_{0.2\%}N_{20\%}$–TiO_2 samples, respectively. Compared to the differences in the particle sizes exhibited for the increase in La (Table 1), it is evident that La has a greater ability to inhibit particle growth than N.

Whether the La/N-doping occurred by replacement or by embedding the space, it caused a corresponding micro-strain in the TiO_2 lattice, accompanied by a change in the crystallinity. The data in Table 1 showed that a certain amount of La-doping effectively restrained the grain growth of TiO_2., The smallest grain size of only 10.7 nm was obtained when nLa: nTi was 0.15% whereas the undoped crystal particle was 17.1 nm. Smaller grains can increase the nano-TiO_2 surface area and can increase the surface oxygen vacancies and concentration of defects, which are conducive to the separation of photo-electrons and holes. However, excess dopant (nLa: nTi = 0.2%) may causes serious lattice distortion, decrease numbers of defects, fewer oxygen holes and increased the grain size.

3.1.2. Raman spectra

The Raman spectra of the undoped, La_x/TiO_2 and La_xN_y/TiO_2 obtained after calcination at 500 °C are measured at room temperature. Optical Raman spectroscopy is a powerful tool in the study of TiO_2 because of its high sensitivity to microstructure. Fig. 2 shows peaks at 144 cm^{-1}, 400.3 cm^{-1}, 517.5 cm^{-1} and 638 cm^{-1}, which are assigned, respectively, to the E_g, B_{1g}, A_{1g}, and Eg vibrational modes of the anatase phase [34,35]. The absence of Raman bands (235, 447 and 612 cm^{-1}) corresponding to the rutile phase of titania reconfirms the phase purity of our sample [36]. Compared with pure TiO_2, the $La_{0.2\%}/TiO_2$ and $La_{0.2\%}N_{20\%}/TiO_2$ peak widths exhibit more obvious changes, indicating that doping with La^{3+} ions plays an important role in reducing the dimension of the TiO_2 crystallites and indicating that the synergistic effects of co-doping TiO_2 with La and N further decrease the size of the crystal particles. $La_{0.2\%}N_{20\%}/TiO_2$ shows a significant decrease in the intensity of the Raman bands compared to $La_{0.2\%}/TiO_2$. The results also indicate that doping with La ions shifts the absorption slightly towards higher wave numbers. The shift in the doped TiO_2 could be indicative of structural changes caused either by interstitial or substitutional impurities [37].

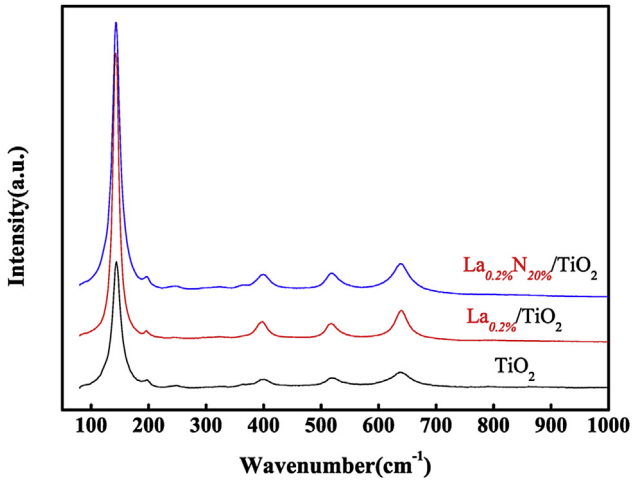

Fig. 2. Raman spectra of $La_{0.2\%}N_{20\%}/TiO_2$, $La_{0.2\%}/TiO_2$ and TiO_2 film electrodes calcined at 500 °C.

3.1.3. Diffuse reflectance spectra (DRS)

Fig. 3a shows the UV–Vis DRS absorption spectra of $La_{0.2\%}N_{20\%}/TiO_2$, $La_{0.2\%}/TiO_2$, $N_{20\%}/TiO_2$ and TiO_2 As seen, compared with the TiO_2 sample, the $La_{0.2\%}N_{20\%}/TiO_2$, $La_{0.2\%}/TiO_2$, $N_{20\%}/TiO_2$ samples have large humps at approximately 450 nm, 469 nm and 480 nm, respectively. This obvious extension of the edge of the adsorption spectrum into the visible light region could be ascribed to the introduction of both N and La into TiO_2. $La_{0.2\%}/TiO_2$ and $La_{0.2\%}N_{20\%}/TiO_2$ are also found to show more absorption, greater extension into the visible light region and narrower band gaps. The amount of red shift in the samples is $La_{0.2\%}N_{20\%}/TiO_2$ > $La_{0.2\%}/TiO_2$ > $N_{20\%}/TiO_2$ > TiO_2.

To further study the change in the band gap of the $La_{0.2\%}N_{20\%}/TiO_2$, $La_{0.2\%}/TiO_2$, $N_{20\%}/TiO_2$ and TiO_2 film electrodes, the band gaps were estimated with the following equation: $(\alpha h\nu) = A\,(h\nu - E_g)^n$, where α, E_g, h, ν, n and A are the absorption coefficient; the band gap (eV); Planck's constant (6.6260×10^{-34} J s); the frequency of light (s^{-1}); a number characterizing the transition, which is n = ½ for TiO_2 and a constant, respectively [33]. The band gap was estimated by extrapolating tangent lines on the plot of $(\alpha h\nu)^{1/n}$ as a function of $h\nu$ and is shown in Fig. 3b. The results indicate that the band gap energies of $La_{0.2\%}N_{20\%}/TiO_2$, $La_{0.2\%}/TiO_2$ and $N_{20\%}/TiO_2$ are 2.79 eV, 2.98 eV, and 3.09 eV, respectively.

La doping could occur through the substitution of La^{3+} in the La_2O_3 lattice by Ti^{4+} and the formation of vacancies, thus most likely causing an impurity state in the TiO_2 band gap. The existence of an impurity state improves the absorption of visible light by narrowing the band gap of TiO_2. As the absorption edges shift to the red (in web version), the $N_{20\%}/TiO_2$ can absorb visible light. The synergistic effects made the absorption edge of the lanthanum and nitrogen co-doped TiO_2 shift significantly into the visible-light region, and this shift is favourable for improving photocatalytic activity in visible light.

3.1.4. Analysis of FTIR

The FT–IR spectra of the pure TiO_2 and La_xN_y co-doped TiO_2 from 500 to 4000 cm^{-1} are shown in Fig. 4. All of the samples exhibit peaks corresponding to the stretching vibrations of the surface-bonded O–H group and the hydrogen-bonded molecular water species at 3426–3446 cm^{-1}. Peaks observed in the samples at approximately 1630–1638 cm^{-1} are attributed to the vibrational bending of the O–H–O groups on the surface of the sample. The absorption peak at 960 cm^{-1} is associated with the formation of Ti–O–C bridges because of the interaction between the Ti–O bond and the C=O bond.

The absorption peak at 730 cm^{-1} shifted to lower wave numbers because of the Ti–O–La bridges. The vibrational modes of the anatase skeletal O–Ti–O bonds were observed in the range of 500–600 cm^{-1}. The peak at 3426–3446 cm^{-1} reflects the hydroxyl groups adsorbed on the surface as the La dopes the TiO_2; this peak verifies that La doping is beneficial for the absorption of hydroxyl groups on the surface of TiO_2 and consequently improve the photocatalytic activity of the samples.

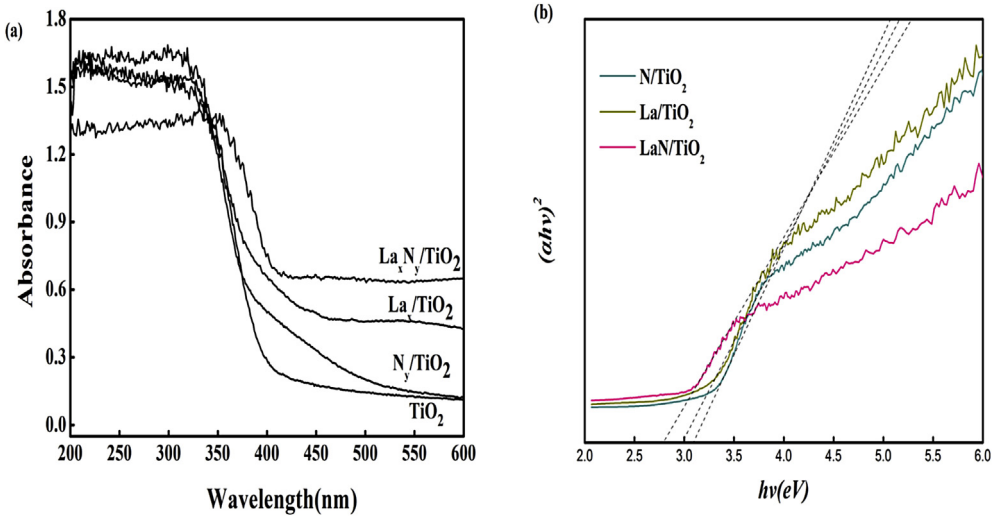

Fig. 3. (a) UV–Vis diffuse reflectance spectra of different samples and (b) plot of transformed Kubelka–Munk function as a function of the energy of the light absorbed.

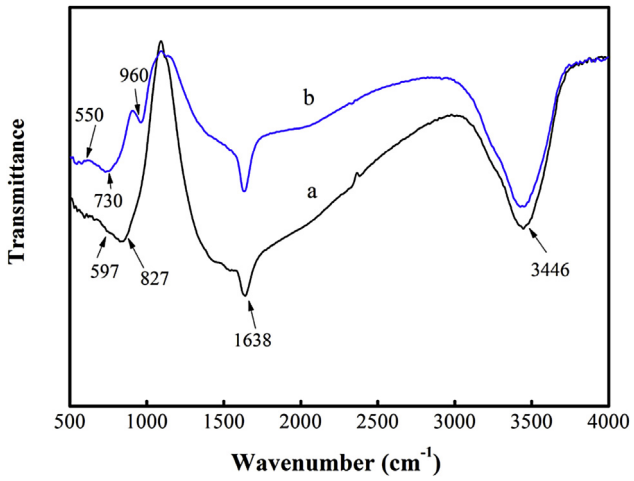

Fig. 4. FT-IR spectra of (a) TiO_2 and (b) $La_{0.2\%}N_{20\%}$ co-doped TiO_2.

3.1.5. SEM

Upon visual observation, the raw Ni foam substrate was light grey in colour; the TiO_2(Ni), La_xN_y/TiO_2(Ni), La_x/TiO_2(Ni) and N_y/TiO_2(Ni) electrodes calcined at 500 °C was celadon, The morphologies of the raw Ni substrate and the doped TiO_2 coating on the Ni foam substrate were examined by SEM, and the SEM images are shown in Fig. 5a and b. Fig. 5a shows that the raw Ni foam substrate has a uniform framework, a smooth surface, a high specific surface area and an even aperture distribution. These results show that the Ni foam substrate is the carrier for the TiO_2 and the doped TiO_2. Furthermore, the Ni foam substrate can be used as a photoanode in photoelectrocatalytic (PEC) processes because of its excellent electrical conductivity. The surface of the Ni foam substrate was found to be rougher than that of the raw Ni substrate in Fig. 5b. The TiO_2 and the doped TiO_2 films are thicker at the edge of the aperture of the Ni foam substrate because the TiO_2 sol clumps together during the TiO_2 coating process. Stress from the lateral contraction of the TiO_2 films is a significant cause of cracking in films calcined at 500 °C. The TiO_2 films warp towards at the cracks and the cracks grow larger. These results indicate that the cracks in the film at the edge of the aperture of the Ni foam substrate are vulnerable in the combined Ni foam substrate and TiO_2 film and significantly affect the service life of the combined system.

3.2. Photoelectrocatalytic activity

3.2.1. Photocatalytic, photoelectrocatalytic and electrocatalytic activities and durability under visible light

The photocatalytic activities of the pure TiO_2, $La_{0.2\%}/TiO_2$, $N_{20\%}/TiO_2$ and $La_{0.2\%}N_{20\%}$ co-doped TiO_2 systems were assessed through the degradation of 30 mg/L aqueous solutions of MG under irradiation with visible light, as shown in Fig. 6a.

We evaluated the photoelectrocatalytic capabilities of TiO_2, $La_{0.2\%}/TiO_2$, $N_{20\%}/TiO_2$ and $La_{0.2\%}N_{20\%}$ co-doped TiO_2. As shown in Fig. 6b, under a bias voltage of 4 V, the PEC and PC (photocatalytic) degradation processes of the TiO_2, $La_{0.2\%}/TiO_2$, $N_{20\%}/TiO_2$ and $La_{0.2\%}N_{20\%}$ co-doped TiO_2 were fit to pseudo-first-order kinetics using the linear transform formula $\ln(C_t/C_0) = kt$, and the values of the apparent rate constant k are shown in Table 2. The $La_{0.2\%}/TiO_2$, $N_{20\%}/TiO_2$ and $La_{0.2\%}N_{20\%}$ co-doped TiO_2 showed higher PEC activity toward the degradation MG than did the TiO_2 film electrode as a synergistic result of the large specific surface areas and the enhanced mass transfer and electron transfer. Furthermore, the visible-light activity of the PC and PEC was clearly observed from the MG degradation. The $La_{0.2\%}N_{20\%}$ co-doped TiO_2 possessed the best photocatalytic activity. The $La_{0.2\%}N_{20\%}$ co-doped TiO_2 possessed the best PEC activity because the slow photon effect contributed to the degradation process when the bias voltage was applied.

The photoelectrocatalytic stability of $La_{0.2\%}N_{20\%}$ co-doped TiO_2(Ni) under visible light was also evaluated by recycling the photo-electrode in the degradation of MG, and the result is shown in Fig. 7. After being used five times, the removal efficiency of the $La_{0.2\%}N_{20\%}$ co-doped TiO_2(Ni) for MG remains above 80%. These results indicate that a photo-electrode of $La_{0.2\%}N_{20\%}$ co-doped TiO_2(Ni) possesses not only high photocatalytic activity but also has good stability.

3.2.2. Effect of applied electrical potential on PEC oxidation

As shown in Fig. 8a, to study the effect of the electrical bias voltage on the PEC degradation of MG, different bias voltages(V) of 0, 2,3, 4, 5, 6 and 7 V were investigated with the $La_{0.2\%}N_{20\%}$ co-doped TiO_2(Ni) electrode with the same light intensity of 80.4 mW cm^2 and at the same pH 7 for the MG degradation. The results showed

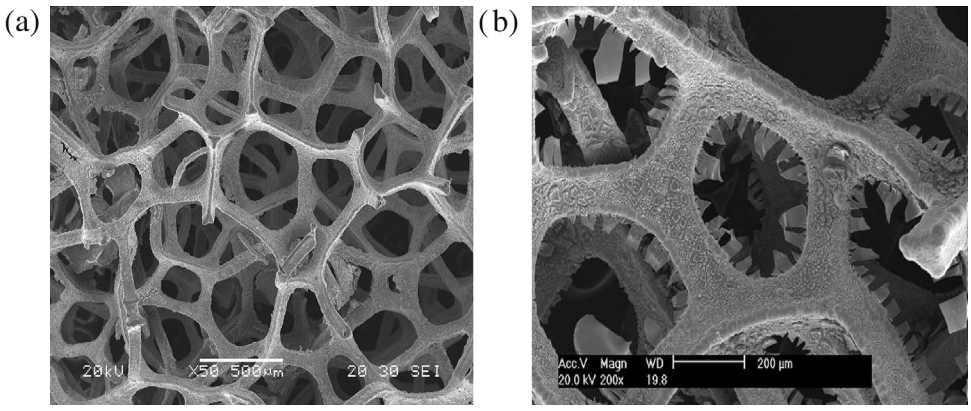

Fig. 5. (a) SEM image of nickel foam substrate and (b) La_xN_y/TiO_2 immobilized on nickel foam substrate.

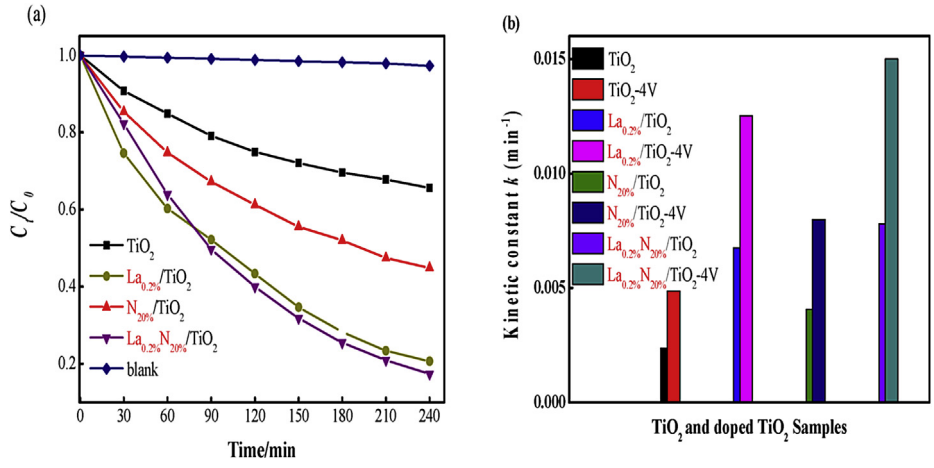

Fig. 6. (a) Photocatalytic degradation of MG for different samples and (b) the kinetic constants (k) for different samples during PEC and photocatalytic degradation under irradiation with visible light.

Table 2
Apparent rate constants k of different samples during PEC and PC degradation under irradiation with visible light.

Process	TiO_2	$La_{0.2\%}/TiO_2$,	$N_{20\%}/TiO_2$	$La_{0.2\%}N_{20\%}$ co-doped TiO_2
Photocatalytic	0.00238	0.00676	0.00407	0.0078
Photoelectrocatalytic-4 V	0.00486	0.01252	0.00798	0.015

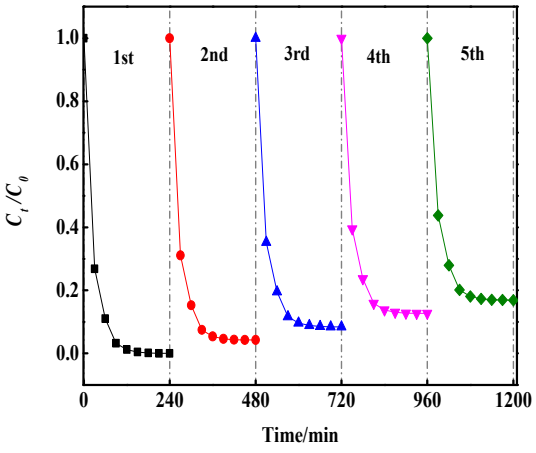

Fig. 7. Degradation of MG (30 mg/L) with a recycled $La_{0.2\%}N_{20\%}$ co-doped TiO_2(Ni) electrode under visible light.

that when the applied voltage was increased from 0 to 4 V, the degradation ratio of MG increased rapidly from 81.3% to 99.9%. However, when the applied voltage increased further to 5 V, the degradation ratio was slightly reduced.

The results showed that 4 V may be an optimal voltage for the PEC degradation of MG. When the bias voltage was lower than 4 V, the first-order kinetic constant k increased as the bias voltage increased. When the bias voltage was higher than 4 V, the first-order kinetic constant k decreased as the bias voltage increased. As shown in Fig. 8b, there was a parabolic relationship ($R^2 = 0.9833$) between the bias voltage (V) and the first-order kinetic constants k, described by Eq. (1), where 0.0078 represents the average value of k for a light intensity of 80.4 mW cm^2 and at pH 7. According to Eq. (1), the optimal bias voltage to achieve the maximum k value is 4.58 V.

$$k' = 0.00837V^2 - 0.000907143V - 0.00512 \quad (1)$$

In this study, we propose that the first-order kinetic coefficient

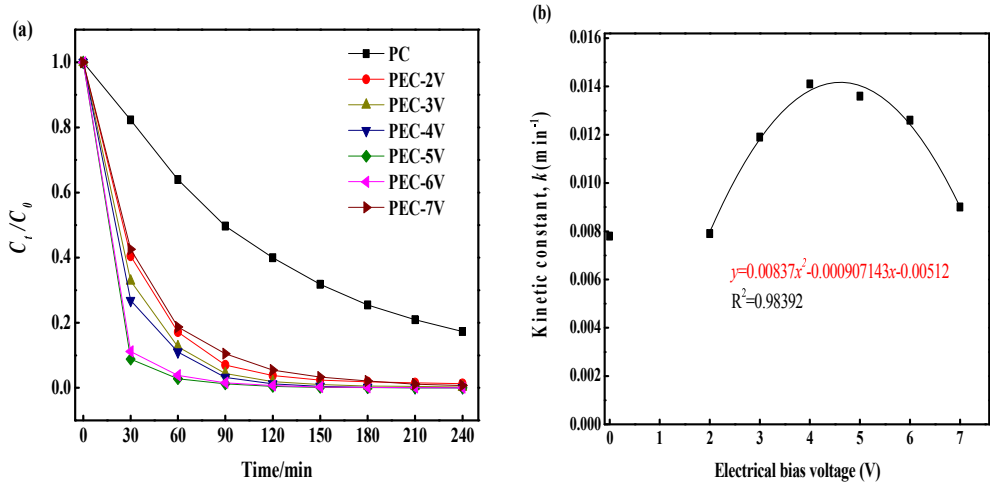

Fig. 8. (a) The photoelectrocatalytic degradation of MG at different electrical bias voltages and (b) the first-order kinetic constant k as a function of the electrical bias voltage.

(k_0) is a function of the bias voltage (V) when the bias voltage is below its optimal value of 4.58 V.

3.3. Mechanistic considerations

Based on the experimental results, the enhanced photocatalytic activity can be attributed to the synergistic effects of the co-doping TiO_2 with lanthanum and nitrogen ions. On one hand, the N 2p energy level is situated above the valence band and will decrease the band gap of the pure TiO_2 and improve the photocatalytic activity in the visible light region. Under irradiation with the visible light, photo-generated electrons and holes were produced by photons. The electrons are captured by O_2 adsorbed on the surface to form O_2^-, which can react with the organic pollutants. The holes react with OH^-or H_2O to form hydroxyl radicals (•OH), which can strongly oxidize and destroy the organic molecules. Conversely, substitutional and interstitial doping are two types of doping modes for La^{3+}. From the data in Table 1, the crystalline size of La^{3+}-doped TiO_2 is observed to be smaller than that of pure TiO_2. It is reasonable to suppose that a small portion of the La^{3+} ions enter site inside the TiO_2 and the rest occupy places on the surface, in the interstitial TiO_2 positions and form Ti—O—La bonds. Because the La—O chemical bond is stronger than the Ti—O bond, it will produce an oxygen vacancy and create a charge imbalance, which results in the increased adsorption of hydroxide ions onto the surface of co-doped TiO_2 to maintain charge balance. The hydroxyl ions not only inhibit electron hole recombination, thereby increasing the lifetime of the charge carriers, but also react with the photo-generated holes to produce hydroxyl radicals during irradiation. The La dopant may act as a sink to trap the excited electrons or may introduce an impurity band in the band gap of TiO_2; this impurity band can either accept an electron from the valence band or donate an electron to the conduction band. Visible light has enough energy to promote electrons because of decreased separation between the new energy levels and the valence band or conduction band.

Mechanisms for the photocatalytic and PEC degradation of MG on the La_xN_y co-doped TiO_2(Ni) film electrodes were proposed. In the photocatalytic process, when the La_xN_y co-doped TiO_2(Ni) film electrodes was excited by photons, electrons and holes were generated. The photo-generated holes on the La_xN_y co-doped TiO_2(Ni) film electrodes directly oxidized water to generate hydroxyl radicals, and the excited electrons reacted with the O_2 adsorbed on the surface of the La_xN_y co-doped TiO_2(Ni) film electrodes to generate O_2^-. However, the high recombination rate of electron—hole pairs still hindered the photocatalytic efficiency of MG degradation.

The photocatalytic degradation of dyes on the co-doped TiO_2 under visible light irradiation can be explained in terms of the following equations (2)—(5):

$$La_xN_y\text{co}-\text{doped}/TiO_2 + h\nu \rightarrow e_{cb}^- + h_{vb}^+ \quad (2)$$

$$O_2 + e_{cb}^- \rightarrow O_2^{\cdot -} \quad (3)$$

$$H_2O + h_{vb}^+ \rightarrow H^+ + \cdot OH \quad (4)$$

$$\cdot OH\ /O_2^{\cdot -}\ /h_{vb}^+ + \text{organic/dyes} \rightarrow \text{deg raded products} \quad (5)$$

In contrast, in the PEC system, the photo-generated electrons in the excited La_xN_y co-doped TiO_2(Ni) film electrodes were removed to the graphite electrode by the electric field. Meanwhile, the photo-generated holes remained at the surface of the La_xN_y co-doped TiO_2(Ni) film electrodes to improve the efficiency of oxidation, which was the main source of hydroxyl radicals. Additionally, the injected electrons reacted with the O_2 adsorbed on the surface of the graphite electrode and the removed photo-generated electrons reacted with the O_2 adsorbed on the surface of the La_xN_y co-doped TiO_2(Ni) electrode to create $O_2^{\cdot -}$. The PEC process solved the problem of the recombination of photo-generated electron—hole pairs in the PC process (Eqs. (2)—(5)), and the co-doping was beneficial for the active species, such as ·OH and O_2^- (Eq. (7) and (8)).

In the PEC system, the anode reaction is:

$$La_xN_y\text{co}-\text{doped}/TiO_2 + h\nu(>E_g) \rightarrow e_{cb}^- + h_{vb}^+ \quad (6)$$

$$O_2 + e_{cb}^- \rightarrow O_2^{\cdot -} \quad (7)$$

$$H_2O + h_{vb}^+ \rightarrow H^+ + \cdot OH \quad (8)$$

$$La_xN_y\text{co}-\text{doped}/TiO_2\left(e_{cb}^-\right) + \text{external electrostatic field} \rightarrow \text{external circuit} \quad (9)$$

The cathode reaction is:

$$O_2 + e_{cb}^- \rightarrow O_2^{\cdot -} \quad (10)$$

$$\cdot OH\ /O_2^{\cdot -}\ \Big/ h_{vb}^+ + \text{organic/dyes} \rightarrow \text{deg raded products} \quad (11)$$

4. Conclusions

In conclusion, La_xN_y co-doped TiO_2(Ni) film electrodes were successfully synthesized by sol–gel and dip-coating methods. Analysis of the characteristics of these electrodes showed that the co-doping notably affected the structure and the photocatalytic activity of the TiO_2. Nitrogen doping can narrow the band gap of TiO_2 and enhance the utilization efficiency of visible light whereas La^{3+} doping can promote the separation of photoelectrons and holes. TiO_2 co-doped with lanthanum and nitrogen exhibited much higher photocatalytic activity in the visible light region than pure TiO_2, nitrogen-doped TiO_2 and La- doped TiO_2 with the same doping condition; this result was ascribed to the small crystal size, the prevention of the phase transition from the anatase to rutile phase and the slow recombination rate of the photo-generated electrons and holes. La and N co-doping could produce synergistic effects.

PEC provided a solution to the difficult problem of recombination between photogenerated electron–hole pairs. Because of the co-doping in TiO_2, the potential bias applied to the La_xN_y co-doped TiO_2(Ni) photo-anode strengthened the photocatalytic efficiency of the La_xN_y co-doped TiO_2(Ni) electrode. The La_xN_y co-doped TiO_2(Ni) electrode exhibited even better PEC activity than the TiO_2 electrode toward the degradation of MG under irradiation visible light by applying a bias voltage of 4 V. Furthermore, the La_xN_y co-doped TiO_2(Ni) electrode showed different properties in the PEC and photocatalytic degradation of MG.

Finally, two degradation mechanisms for the La_xN_y co-doped TiO_2(Ni) film electrodes in PEC and photocatalytic systems were proposed. This study on the La_xN_y co-doped TiO_2(Ni) film electrode affords a feasible method for the development of a photo-anode with visible light photoelectrocatalytic activity that is promising for environmental applications.

Acknowledgements

The authors wish to gratefully acknowledge financial support from the National Natural Science Foundation (21277052), the Department of Guangdong Education and Science and Technology Bureau (2010), the State Key Laboratory of Subtropical Building Science (2013ZC03, 2014ZB04, 2016ZB24), the Environmental Protection Bureau (201203), the Guizhou Province Scientific Technology Foundation (20152056), the Guizhou Academy of Sciences Foundation for Young Scientists(Grant No. 019) and the Guizhou Talent Base Foundation. The authors would like to acknowledge assistance from the staffs who provided full support for this study. Moreover, the authors would like to express their sincere appreciation to the anonymous reviewers for their helpful comments and suggestions.

References

[1] Lin X, Rong F, Ji X, Fu D. Carbon-doped mesoporous TiO_2 film and its photocatalytic activity. Microporous Mesoporous Mater 2011;142(1):276–81.
[2] Tung WS, Daoud WA. New approach toward nanosized ferrous ferric oxide and Fe_3O_4-doped titanium dioxide photocatalysts. ACS Appl Mater Interfaces 2009;1(11):2453–61.
[3] Zhu JF, Zheng W, Bin HE, Zhang JL, Anpo M. Characterization of Fe-TiO_2 photocatalysts synthesized by hydrothermal method and their photocatalytic reactivity for photodegradation of XRG dye diluted in water. J Mol Catal A Chem 2004;216(1):35–43.
[4] Liu J, Si R, Zheng H, Geng Q, Dai W, Chen X, et al. The promoted oxidation of CO induced by the visible-light response of Au nanoparticles over Au/TiO_2. Catal Commun 2012;26:136–9.
[5] Oros-Ruiz S, Gomez R, Lopez R, Hernandez-Gordillo A, Pedraza-Avella JA, Moctezuma E, et al. Photocatalytic reduction of methyl orange on Au/TiO_2 semiconductors. Catal Commun 2012;21:72–6.
[6] Ismail AA. Facile synthesis of mesoporous Ag-loaded TiO_2 thin film and its photocatalytic properties. Microporous Mesoporous Mater 2012;149(1):69–75.
[7] Jing LQ, Sun XJ, Xin BF, Wang BQ, Cai WM, Fu HG. The preparation and characterization of La doped TiO_2 nanoparticles and their photocatalytic activity. J Solid State Chem 2004;177(10):3375–82.
[8] Xie YB, Yuan CW. Visible-light responsive cerium ion modified titania sol and nanocrystallites for X-3B dye photodegradation. Appl Catal B Environ 2003;46(2):251–9.
[9] Xu J, Ao Y, Fu D, Yuan C. Low-temperature preparation of F-doped TiO_2 film and its photocatalytic activity under solar light. Appl Surf Sci 2008;254(10):3033–8.
[10] Li X, Huang Y, Chen J-F, Tao X. Visible light-driven binary dyes synergic degradation by iodine-doped TiO_2 nanocrystal film. Catal Commun 2012;20:94–8.
[11] Ang TP, Law JY, Han Y-F. Preparation, characterization of sulfur-doped nanosized TiO_2 and photocatalytic degradation of methylene blue under visible light. Catal Lett 2010;139(1–2):77–84.
[12] Xiang Q, Yu J, Wang W, Jaroniec M. Nitrogen self-doped nanosized TiO_2 sheets with exposed {001} facets for enhanced visible-light photocatalytic activity. Chem Commun 2011;47(24):6906–8.
[13] Bae E, Choi W. Highly enhanced photoreductive degradation of perchlorinated compounds on dye-sensitized metal/TiO_2 under visible light. Environ Sci Technol 2003;37(1):147–52.
[14] Yu JG, Yu HG, Cheng B, Zhao XJ, Yu JC, Ho WK. The effect of calcination temperature on the surface microstructure and photocatalytic activity of TiO_2 thin films prepared by liquid phase deposition. J Phys Chem B 2003;107(50):13871–9.
[15] Li YX, Me YZ, Peng SQ, Lu GX, Li SB. Photocatalytic hydrogen generation in the presence of chloroacetic acids over Pt/TiO_2. Chemosphere 2006;63(8):1312–8.
[16] Zhang X, Zhou G, Zhang H, Wu C, Song H. Characterization and activity of visible light-driven TiO_2 photocatalysts co-doped with nitrogen and lanthanum. Transit Metal Chem 2011;36(2):217–22.
[17] Li J, Xu J, Dai W-L, Li H, Fan K. One-pot synthesis of twist-like helix tungsten-nitrogen-codoped titania photocatalysts with highly improved visible light activity in the abatement of phenol. Appl Catal B Environ 2008;82(3–4):233–43.
[18] Asahi R, Morikawa T, Ohwaki T, Aoki K, Taga Y. Visible-light photocatalysis in nitrogen-doped titanium oxides. Science 2001;293(5528):269–71.
[19] Devi LG, Kavitha R. Review on modified N-TiO_2 for green energy applications under UV/visible light: selected results and reaction mechanisms. RSC Adv 2014;4(54):28265–99.
[20] Umebayashi T, Yamaki T, Itoh H, Asai K. Analysis of electronic structures of 3d transition metal-doped TiO_2 based on band calculations. J Phys Chem Solids 2002;63(10):1909–20.
[21] Gai Y, Li J, Li S-S, Xia J-B, Wei S-H. Design of Narrow-Gap TiO_2: a passivated codoping approach for enhanced photoelectrochemical activity. Phys Rev Lett 2009;102(3).
[22] Cong Y, Tian B, Zhang J. Improving the thermal stability and photocatalytic activity of nanosized titanium dioxide via La^{3+} and N co-doping. Appl Catal B Environ 2011;101(3–4):376–81.
[23] He C, Li XZ, Graham N, Wang Y. Preparation of MATO and TiO_2/Ti photoelectrodes by magnetron sputtering for photocatalytic application. Appl Catal A General 2006;305(1):54–63.
[24] Hou Y, Qu J, Zhao X, Lei P, Wan D, Huang CP. Electro-photocatalytic degradation of acid orange II using a novel TiO_2/ACF photoanode. Sci Total Environ 2009;407(7):2431–9.
[25] Li XZ, Liu HL, Yue PT, Sun YP. Photoelectrocatalytic oxidation of rose bengal in aqueous solution using a Ti/TiO_2 mesh electrode. Environ Sci Technol 2000;34(20):4401–6.
[26] Grosso D. How to exploit the full potential of the dip-coating process to better control film formation. J Mater Chem 2011;21(43):17033–8.
[27] Comparelli R, Fanizza E, Curri ML, Cozzoli PD, Mascolo G, Passino R, et al. Photocatalytic degradation of azo dyes by organic-capped anatase TiO_2 nanocrystals immobilized onto substrates. Appl Catal B Environ 2005;55(2):81–91.
[28] Mascolo G, Comparelli R, Curri ML, Lovecchio G, Lopez A, Agostiano A. Photocatalytic degradation of methyl red by TiO_2: comparison of the efficiency of immobilized nanoparticles versus conventional suspended catalyst. J Hazard Mater 2007;142(1–2):130–7.
[29] Xing M, Zhang J, Chen F. New approaches to prepare nitrogen-doped TiO_2 photocatalysts and study on their photocatalytic activities in visible light. Appl Catal B Environ 2009;89(3–4):563–9.
[30] Vinodgopal K, Hotchandani S, Kamat PV. Electrochemically assisted photocatalysis: titania particulate film electrodes for photocatalytic degradation of 4-chlorophenol. J Phys Chem 1993;97(35):9040–4.
[31] Paschoal FMM, Anderson MA, Zanoni MVB. The photoelectrocatalytic oxidative treatment of textile wastewater containing disperse dyes. Desalination 2009;249(3):1350–5.

[32] Zhou X, Zheng Y, Liu D, Zhou S. Photoelectrocatalytic degradation of humic acids using codoped TiO_2 film electrodes under visible light. Int J Photoenergy 2014.
[33] Ohsaka T, Izumi F, Fujiki Y. Raman spectrum of anatase, TiO_2. J Raman Spectrosc 1978;7(6):321–4.
[34] Hsien YH, Chang CF, Chen YH, Cheng SF. Photodegradation of aromatic pollutants in water over TiO_2 supported on molecular sieves. Appl Catal B Environ 2001;31(4):241–9.
[35] Chan SS, Wachs IE, Murrell LL, Wang L, Hall WK. In situ laser Raman spectroscopy of supported metal oxides. J Phys Chem 1984;88(24):5831–5.
[36] Li H, Zhang X, Huo Y, Zhu J. Supercritical preparation of a highly active s-doped TiO_2 photocatalyst for methylene blue mineralization. Environ Sci Technol 2007;41(12):4410–4.
[37] Sibu CP, Kumar SR, Mukundan P, Warrier KGK. Structural modifications and associated properties of lanthanum oxide doped sol-gel nanosized titanium oxide. Chem Mater 2002;14(7):2876–81.